mathematics

IMPACT FACTOR 2.3

CITESCORE 4.0

Article

A Non-Relativistic 2D Quantum System and Its Thermo-Magnetic Properties with a Generalized Pseudo-Harmonic Oscillator

Haifa I. Alrebdi, Akpan N. Ikot, Ridha Horchani and Uduakobong S. Okorie

MDPI

https://doi.org/10.3390/math12172623

mathematics

Article

A Non-Relativistic 2D Quantum System and Its Thermo-Magnetic Properties with a Generalized Pseudo-Harmonic Oscillator

Haifa I. Alrebdi [1], Akpan N. Ikot [2,3,*], Ridha Horchani [4,*] and Uduakobong S. Okorie [5,6]

1 Department of Physics, College of Science, Princess Nourah bint Abdulrahman University, P.O. Box 84428, Riyadh 11671, Saudi Arabia; hialrebdi@pnu.edu.sa
2 Theoretical Physics Group, Department of Physics, University of Port Harcourt, Choba, Port Harcourt 500004, Nigeria
3 Western Caspian University, Baku 1001, Azerbaijan
4 Department of Physics, College of Science, Sultan Qaboos University, P. C. 123, Al-Khod, Muscat P.O. Box 36, Oman
5 Department of Physics, University of South Africa, Florida Campus, Johannesburg 1710, South Africa; uduakobongokorie@aksu.edu.ng
6 Department of Physics, Akwa Ibom State University, Ikot Akpaden, P. M. B. 1167, Uyo 520221, Nigeria
* Correspondence: akpan.ikot@uniport.edu.ng (A.N.I.); horchani@squ.edu.om (R.H.)

Abstract: In this work, we examine the thermo-magnetic characteristics and energy spectra of a system exposed to both magnetic and Aharonov–Bohm (AB) fields with the existence of an interaction potential that is pseudo-harmonic. Explicit calculations of the eigen-solutions are performed with the expanded Nikiforov–Uvarov formalism. The confluent Heun function is used to represent the equivalent wave functions. If the AB and magnetic fields are gone, quasi-degeneracy in the system's energy levels is shown by a numerical analysis of the energy spectrum. Additionally, we provided a visual representation of how the AB and magnetic fields affected the system's thermo-magnetic characteristics. Our results show a strong dependence of thermo-magnetic properties on temperature, screening parameters, external magnetic fields, and AB fields.

Keywords: energy spectra; thermo-magnetic properties; confluent Heun function; extended Nikiforov–Uvarov (ENU) method

MSC: 80A05; 81S05; 82B30; 82D40

Citation: Alrebdi, H.I.; Ikot, A.N.; Horchani, R.; Okorie, U.S. A Non-Relativistic 2D Quantum System and Its Thermo-Magnetic Properties with a Generalized Pseudo-Harmonic Oscillator. *Mathematics* **2024**, *12*, 2623. https://doi.org/10.3390/math12172623

Academic Editor: Davide Valenti

Received: 29 July 2024
Revised: 15 August 2024
Accepted: 20 August 2024
Published: 24 August 2024

1. Introduction

The transition from the three-dimensional non-relativistic equation to the two-dimensional (2D) non-relativistic equation, which involves external magnetic fields, is achieved by mapping the momentum operator as $\vec{P} \to \left(\vec{P} - \frac{e}{c}\vec{A}\right)$, where $\vec{A}$ is a vector field affected by either external magnetic, AB forces, or both; $\vec{P} \to i\hbar\vec{\nabla}$ is the momentum operator; and $\hbar$, c and e have their usual meanings [1–5]. The eigen-solutions of the 2D can be mapped into 3D and not vice versa. Therefore, the 2D non-relativistic quantum mechanics for particles moving and influenced by physical potential fields have enormous applicability in several fields of physics. Also, if the eigen-solutions of the Schrodinger-like equation (SE) with applicable solvable potential are known, then the quantum dynamics of the particles can be investigated, such as thermo-magnetic properties [6–8], mass spectra [9–11], quantum dots [12–16], thermodynamic properties [17–20], theoretic information theory [21–25], optical properties [26–30], among others. In addition, the eigen-solutions of the 2D Schrodinger equations (2D-SEs) have been used in the study of confinement in quantum dots and interband transitions in quantum pseudodots [31–33]. In one of the investigations, Filgueiras et al. [34] determined the energy spectra and eigenfunction for 2D pseudo-harmonic quantum dots influenced by screw dislocation. The Dirac particles in 2D with modified Pöschl–Teller potential interaction have been investigated by Ferkous et al. [35].

Numerous researchers have made significant efforts to solve the 2D-SE interacting with solvable potential models. For example, studies have been conducted on the 2D-SE with a Hulthen potential when there is an AB field [36]. Similarly, Eshghi et al. [37] have studied the Schrödinger equation in two dimensions for a particle with electric charge interacting with mass-dependent Morse-plus-Coulomb potentials.

The 2D-SE eigen-solutions with the screened Kratzer potential have been examined by Ikot et al. [38]. Ikhdair et al. have examined the SE solutions employing an AB field and a constant magnetic field [39]. Additional reports have discussed how the hydrogen atom is affected by AB, magnetic, and electric fields. Horchani et al. [40] investigated the magnetic properties and energy spectra of a 2D-SE with an inverse square potential. Khordad and Sedehi [41] examined the system's thermodynamic properties while examining the 2D-SE for a quantum dot with double ring-shaped potential. Vicente et al. [42] expanded on the work of Khordad and Sedehi. Other applications of the 2D-SE include the study of energy spectra, magnetic fields [43], and entropy. Khordad and Sedeh [31] used the Tsallis entropy formulation, both extensive and non-extensive, in noncommutative phase space quantum mechanics to determine the magnetic susceptibility of graphene. Ibragimov [44] used a 2D non-relativistic framework to study the thermodynamic features of parabolic quantum dots. In two-dimensional non-relativistic quantum mechanics, the magnetic susceptibility and magnetization of parabolic GaAs quantum dots were calculated by Alia et al. [45].

Recently, numerous researchers have directed considerable attention towards the study of the non-relativistic harmonic oscillator problem. The significant applications of quantum systems with pseudo-harmonic oscillators in atomic, molecular, and chemical physics have led to much research on the topic [13].

The primary objective of this work is to solve the 2D-SE by utilizing the generalized pseudo-harmonic oscillator, defined as [46]

$$V(r) = V_0 e^{2\alpha\rho}\left(1 - e^{-\alpha\rho}\right)^2 + V_1 \frac{e^{-2\alpha\rho}}{\left(1 - e^{-\alpha\rho}\right)} + V_2 \tag{1}$$

where V_0, V_1, and V_2 elucidate the extent of the potential and α shows the screening parameter. Equation (1) is simplified to the widely recognized pseudo-harmonic potential if we map $V_0 \to \frac{a}{\alpha^2}$, $V_1 \to b\alpha^2$, $V_2 \to c$ and take the limit as $\delta \to 0$, with a, b and c being the potential parameters of the pseudo-harmonic oscillator. However, due to the centrifugal barrier term in the 2D-SE, such an equation cannot be solved in an exact form. Thus, an approximation scheme needs to be employed in order to find approximate analytical solutions. The resulting second-order differential equation (DE) arising from the 2D-SE with the generalized pseudo-harmonic oscillator poses another challenge because one of the polynomials is of degree four, which renders well-known analytical techniques such as the Nikiforov–Uvarov (NU) method [47], the factorization method [48], the exact quantization rule [49], the NU Functional Analysis (NUFA) method [50], and supersymmetric quantum mechanics [51] unsuitable for its solutions. Therefore, we will use the extended Nikiforov–Uvarov (ENU) technique [52–54] to solve this equation and study the thermo-magnetic properties, such as F, U, S, C, M, χ, and I, for the generalized pseudo-harmonic oscillator.

The arrangement of the remaining paper is as follows: The expanded NU approach for solving the SE in 2D is explained in Section 2. The theory of the partition function $Z(\beta)$ and thermo-magnetic characteristics are covered in Section 3. The results and comments are presented in Section 4, and Section 5 summarizes the work.

2. Two-Dimensional Schrödinger Equation with a Generalized Pseudo-Harmonic Oscillator

The 2D Schrödinger formula, featuring generalized pseudo-harmonic potential, can be written as [38–40]

$$\left\{\frac{1}{2\mu}\left(i\hbar\vec{\nabla}-\frac{e}{c}\vec{A}\right)^2\right\}\psi(\rho,\varphi)=\left(E_{nm}-V_0e^{2\alpha\rho}\left(1-e^{-\alpha\rho}\right)^2-V_1\frac{e^{-2\alpha\rho}}{\left(1-e^{-\alpha\rho}\right)}-V_2\right)\psi(\rho,\varphi), \quad (2)$$

where μ is the effective mass of the system, E_{nm} denotes the energy level, and $\vec{A}$ is the vector potential, which is given by

$$\vec{A}=\left(0,\frac{Be^{-\alpha\rho}}{\left(1-e^{-\alpha\rho}\right)}+\frac{\phi_{AB}}{2\pi\rho},0\right) \quad (3)$$

where B shows the magnetic field applied externally and Φ_{AB} is the AB field.

To find the analytical solutions of Equation (2), it is essential to use the Laplacian operator expressed in cylindrical coordinates and to use the Greenish–Aldrich approximation scheme to deal with the centrifugal barrier term [55]:

$$\rho^{-2}\approx 4\alpha^2e^{-2\alpha\rho}\left(1-e^{-\alpha\rho}\right)^{-2},\ \rho^{-1}\approx 2\alpha e^{-\alpha\rho}\left(1-e^{-\alpha\rho}\right)^{-1} \quad (4)$$

By substituting Equations (3) and (4) into Equation (2) and performing some algebraic manipulations, Equation (2) transforms into

$$R''_{nm}(\rho)+\left\{\begin{array}{l}\frac{2\mu E}{\hbar^2}-\frac{2\mu V_0}{\hbar^2}e^{2\alpha\rho}\left(1-e^{-\alpha\rho}\right)^2-\frac{2\mu V_1}{\hbar^2}\frac{e^{-2\alpha\rho}}{(1-e^{-\alpha\rho})^2}-\frac{2\mu V_2}{\hbar^2}-\frac{4\alpha^2\left((m+\eta)^2-\frac{1}{4}\right)e^{-2\alpha\rho}}{(1-e^{-\alpha\rho})^2}-\\ \frac{2\alpha\lambda e^{-2\alpha\rho}}{(1-e^{-\alpha\rho})^2}-\frac{\sigma e^{-2\alpha\rho}}{(1-e^{-\alpha\rho})^2}\end{array}\right\}R_{nm}(\rho)=0 \quad (5)$$

using the acronyms listed below:

$$\left.\begin{array}{l}\lambda=\left(\frac{e}{\hbar c}\right)^2\left(\frac{B\Phi_{AB}}{\pi}\right);\ \sigma=\left(\frac{eB}{\hbar c}\right)^2;\ \eta=\frac{\phi_{AB}}{\phi_0};\\ (m+\eta)^2=m^2+\frac{e\Phi_{AB}}{2\pi hc}m+\left(\frac{e\Phi_{AB}}{2\pi hc}\right)^2;\ \phi_0=\frac{2\pi hc}{e}\end{array}\right] \quad (6)$$

and Φ_{AB} is the flux quantum.

By setting $\varepsilon_{nm}=\frac{2\mu(E+V_2)}{\hbar^2}$ and using the following coordinate transformation $x=e^{-\alpha\rho}$, Equation (5) then turns into

$$\frac{d^2R_{nm}(x)}{dx^2}+\frac{x(1-x)}{x^2(1-x)}\frac{dR_{nm}(x)}{dx}+\frac{1}{x^4(1-x)^2}\left\{\begin{array}{l}-\left(\varepsilon_{nm}^2+\xi+\Sigma\right)x^4+\left(2\varepsilon_{nm}^2+4\Sigma\right)x^3\\ -\left(\varepsilon_{nm}^2+6\Sigma\right)x^2+4\Sigma x-\Sigma\end{array}\right\}R_{nm}(x)=0 \quad (7)$$

where

$$\xi=\left(\frac{2\mu V_1}{\hbar^2\alpha^2}+4\left((m+\eta)^2-\frac{1}{4}\right)+\frac{2\lambda}{\alpha}+\frac{\sigma}{\alpha^2}\right);\ \Sigma=\frac{2\mu V_0}{\hbar^2\alpha^2} \quad (8)$$

Equation (7) has three singularities at $x=0,1$ and ∞. It resembles a hypergeometric-type DE, which can be resolved using the ENU method of the form [52–54]

$$\psi''(s)+\frac{\widetilde{\tau}_e(s)}{\sigma_e(s)}\frac{d\psi(s)}{ds}+\frac{\widetilde{\sigma}_e(s)}{\sigma_e{}^2(s)}\psi(s)=0 \quad (9)$$

By comparing Equations (7) and (9), we obtain the following polynomials:

$$\begin{array}{l}\widetilde{\tau}_e(x)=x(1-x),\sigma_e(x)=x^2(1-x),\\ \widetilde{\sigma}_e(x)=-\left(\varepsilon_{nm}^2+\xi+\Sigma\right)x^4+\left(2\varepsilon_{nm}^2+4\Sigma\right)x^3-\left(\varepsilon_{nm}^2+6\Sigma\right)x^2+4\Sigma x-\Sigma\end{array} \quad (10)$$

The $\pi(x)$ function polynomial takes the form

$$\pi(x) = \frac{\sigma_e' - \widetilde{\tau}_e}{2} \pm \sqrt{\left(\frac{\sigma_e' - \widetilde{\tau}_e}{2}\right)^2 - \widetilde{\sigma}_e(x) + G(x)\sigma_e(x)} \tag{11}$$

$$\pi(x) = \frac{x - 2x^2}{2} \pm \left(A + Bx + Cx^2\right) \tag{12}$$

where

$$\begin{aligned} &A = \pm\sqrt{\Sigma}, B = \mp\sqrt{\Sigma}, \\ &C = -(A+B) \pm \sqrt{\tfrac{1}{4} + \xi} \end{aligned} \tag{13}$$

The $G(x)$ value is taken as a linear term of the form $G(x) = Px + Q$. The two position values of the $G(x)$ are given as

$$\begin{aligned} G_1(x) &= Px + Q \\ G_2(x) &= Px - Q \end{aligned} \tag{14}$$

where

$$\begin{aligned} &P = B^2 + 2AC + 2BC + \varepsilon_{nm}^2 - 2\Sigma + \tfrac{3}{4}, \\ &Q = -\varepsilon_{nm}^2 + \xi - 3\Sigma - 2BC - C^2 \end{aligned} \tag{15}$$

From the theory of ENU, we derive the equation $\tau_e(x) = \widetilde{\tau}_e(x) + 2\pi(x)$ as

$$\tau_e(x) = -3x^2 \pm \left(A + Bx + Cx^2\right) \tag{16}$$

We now use the definition

$$H_n = -\frac{1}{2}n\tau' - \frac{n(n-1)}{6}\sigma'' + C_n \tag{17}$$

where C_n is the constant of integration. Thus, we derive the $H_n(x)$ polynomial as

$$H_n(x) = 3nx \mp n(B + 2Cx) - \frac{n(n-1)}{3} + n(n-1)x \tag{18}$$

and its counterpart $H(x) = G(x) + \pi'(x)$ is obtained as

$$H(x) = Px + Q - \frac{1}{2} - 2x \pm (B + 2Cx) \tag{19}$$

By equating $H(x) = H_n(x)$ and setting $C_n = 0$, we determine the eigenvalues of the energy two-dimensional SE with the generalized pseudo-harmonic oscillator as

$$E_{nm} = -V_2 - \frac{\hbar^2\alpha^2\xi}{2\mu} + \frac{3\hbar^2\alpha^2\Sigma}{2\mu} + \frac{\hbar^2\alpha^2}{4\mu} - \frac{\hbar^2\alpha^2 n(n-1)}{6\mu} + \frac{\hbar^2\alpha^2 B(n+1+C)}{2\mu} + \frac{\hbar^2\alpha^2 C^2}{2\mu} \tag{20}$$

where $n = 0, 1, 2 \ldots$

We now proceed to find the wave function. The first component can be calculated by using values $\sigma(x)$ and $\pi(x)$ for $\varphi(x)$ as

$$\varphi(x) = x^A (1-x)^{-(A+B+C-\frac{1}{2})} e^{-(C-1)x} \tag{21}$$

The solution $\chi_n(x)$ is transformed into the confluent Heun differential of the form

$$\chi''(x) + \left[(3-C) + \frac{A}{x} + \frac{A+B+C-3}{1-x}\right]\chi'(x) + \left[\frac{Q+B-\frac{1}{2}}{x} + \frac{P+Q+B+2C-\frac{5}{2}}{1-x}\right]\chi(x) = 0 \tag{22}$$

The function $\chi(x)$ satisfies the confluent Heun DE of the form [55–57]

$$\frac{d^2H(z)}{dz^2}+\left[\alpha'+\frac{\beta'+1}{z}+\frac{\gamma+1}{z-1}\right]\frac{dH(z)}{dz}+\left[\frac{\mu'}{z}+\frac{\nu}{z-1}\right]H(z)=0 \tag{23}$$

The solution of Equation (22) is given as

$$H(z)=Heun\ C\left(\alpha',\beta',\gamma,\delta,\eta;z\right) \tag{24}$$

where $HeunC(\alpha',\beta',\gamma,\delta,\eta,z)$ is the confluent Heun function and the parameters α', β', γ, δ, η are related with μ' and ν as follows:

$$\begin{array}{l}\mu'=\frac{1}{2}(\alpha'-\beta'-\gamma+\alpha'\beta')-\eta\\ v=\frac{1}{2}(\alpha'+\beta'+\gamma+\alpha'\gamma+\beta'\gamma)+\eta+\delta\end{array} \tag{25}$$

Comparing Equations (22) and (23), we obtain

$$\begin{array}{l}\alpha'=(3-C);\ \beta'+1=A;\ \gamma+1=A+B+C-3;\\ \mu'=Q+B-\frac{1}{2};\ \nu=P+Q+B+2C-\frac{5}{2}\end{array} \tag{26}$$

Thus, the solution of Equation (22) becomes

$$\chi_n(x)=Heun\ C\left(\alpha',\beta',\gamma,\delta,\eta;x\right) \tag{27}$$

The entire wave function is obtained as

$$\psi_{n,m}(\rho)=N_n\frac{1}{\sqrt{2\pi\rho}}e^{im\varphi}\left(e^{-\alpha\rho}\right)^A\left(1-e^{-\alpha\rho}\right)^{-\left(A+B+C-\frac{1}{2}\right)}e^{-(C-1)e^{-\alpha\rho}}Heun\ C\left(\alpha',\beta',\gamma,\delta,\eta;e^{-\alpha\rho}\right) \tag{28}$$

where N_n is the normalization constant.

3. Thermo-Magnetic Properties of Generalized Pseudo-Harmonic Oscillator

To investigate the thermo-magnetic characteristics of the system, the initial step involves calculating the partition function $Z(\beta)$, which is defined as [38–40]

$$Z(\beta)=\sum_{n=0}^{\lambda}e^{-\beta E_n},\beta=\frac{1}{k_BT} \tag{29}$$

where β is the inverse temperature parameter, E_n is the energy spectra, and T is the absolute temperature.

In the realm of statistical physics, the $Z(\beta)$ is a fundamental distribution that enables the calculation of various thermomagnetic properties of the system. With respect to Equation (29), once the $Z(\beta)$ is established, key thermomagnetic characteristics like free energy $F(\beta)$, internal energy $U(\beta)$, entropy $S(\beta)$, specific heat capacity $C_v(\beta)$, magnetization $M(\beta)$, magnetic susceptibility $\chi(\beta)$, and persistent current $I(\beta)$ can be systematically computed with the help of the following relations [38–40]:

$$\left.\begin{array}{l}F(\beta)=-\frac{1}{\beta}\ln Z(\beta);\ U(\beta)=-\frac{\partial(\ln Z(\beta))}{\partial\beta};\ S(\beta)=-k_\beta\frac{\partial F(\beta)}{\partial\beta};\ C_v(\beta)=k_\beta\frac{\partial U(\beta)}{\partial\beta};\\ M(\beta)=\frac{1}{\beta}\left(\frac{1}{Z(\beta)}\right)\left(\frac{\partial}{\partial\vec{B}}Z(\beta)\right);\ \chi_m(\beta)=\frac{\partial M(\beta)}{\partial\vec{B}};\ I(\beta)=-\frac{e}{\hbar c}\frac{\partial F(\beta)}{\partial\phi_{AB}}\end{array}\right] \tag{30}$$

4. Results and Discussion

The numerical study of our results for the energy spectra and the thermo-magnetic properties reported in Sections 2 and 3 for the 2D-SE with a generalized pseudo-harmonic oscillator is given in this section. In this study, we investigate the influence of the magnetic and AB fields on the energy spectra and thermodynamic properties of a generalized pseudo-harmonic oscillator. In the numerical computation, we take $V_0 = 2.0$ eV; $V_1 = 3.0$ eV, $V_2 = 3.0$ eV and reduced mass $\mu = 0.5$ eV.

4.1. Energy Spectra

The energy distribution of Equation (20) shows that the electronic state of the generalized pseudo-harmonic system depends on the magnetic field, AB field, and screening parameters. Tables 1–3 display the energy spectrum for the 2D-SE with generalized pseudo-harmonic potential when magnetic and AB fields and the screening parameters are present. Table 1 shows the energy spectra of the pseudo-harmonic oscillator both with and without the AB and magnetic fields. In Table 1, the energy splitting increases in the absence of the AB and magnetic fields at $m = -1, 0, 1$, and one can see in Table 1 that the energy level rises as the values of the principal quantum number n increase. Also, it is evident that in the absence of both magnetic and AB fields (i.e., $B = \Phi_{AB} = 0$ eV), with a screening parameter of $\alpha = 0.5\ ^{-1}$, quasi-degeneracies are observed in the states $E_{0,-1} = E_{0,1} = -0.5002101903687386$ and $E_{1,-1} = E_{1,1} = -0.5502101903368789$, that is, some energy states become degenerate for different values of n and m. Additionally, when either the AB or the magnetic field is absent, the energy levels increase and the spacing between the states also increase. Under these conditions, quasi-degeneracies are observed to occur in two states, and the system's energy levels become less constrained. Conversely, when both fields are present, these degeneracies are removed but some accidental quasi-degeneracies are still present. This clearly shows that the application of the external magnetic fields B and Φ_{AB} removed the degeneracy in the energy levels of the system. When the screening parameters are increased to $0.1\ ^{-1}$ and $0.5\ ^{-1}$, as shown in Tables 2 and 3, respectively, the energy level increased more with increasing screening parameters, and some generate states are observed for different values of n and m.

Table 1. The generalized pseudo-harmonic oscillator's numerical bound state solution under the influence of the AB and magnetic field with a constant magnetic quantum number but a variable principal quantum number for $\alpha = 0.05$.

m	n	**($B = \Phi_{AB} = 0$) eV**	**($B = 0.5$, $\Phi_{AB} = 0$) eV**	**($B = 0$, $\Phi_{AB} = 0.5$) eV**	**($B = 0.5$, $\Phi_{AB} = 0.5$) eV**
0	0	−0.49816948010519724	−0.5486874718707808	−0.4986798170517881	−0.5507784605268133
	1	−0.54816948010519710	−0.5986874718707806	−0.5486798170517879	−0.6007784605268132
	2	−0.59900281343853080	−0.6495208052041144	−0.5995131503851212	−0.6516117938601464
	3	−0.65066948010519710	−0.7011874718707807	−0.6511798170517880	−0.7032784605268132
−1	0	−0.5002101903687386	−0.5506869722180028	−0.4986798170517881	−0.5507784605268133
	1	−0.5502101903687389	−0.6006869722180030	−0.5486798170517879	−0.6007784605268132
	2	−0.6010435237020721	−0.6515203055513363	−0.5995131503851212	−0.6516117938601464
	3	−0.6527101903687385	−0.7031869722180026	−0.6511798170517880	−0.7032784605268132
1	0	−0.5002101903687386	−0.5506869722180028	−0.5027586914629940	−0.5547725285457203
	1	−0.5502101903687389	−0.6006869722180030	−0.5527586914629938	−0.6047725285457206
	2	−0.6010435237020721	−0.6515203055513363	−0.6035920247963276	−0.6556058618790539
	3	−0.6527101903687385	−0.7031869722180026	−0.6552586914629939	−0.7072725285457202

Table 2. The generalized pseudo-harmonic oscillator's numerical bound state solution under the influence of the AB and magnetic field with a constant magnetic quantum number but a variable principal quantum number for $\alpha = 0.10$.

m	n	**($B = \Phi_{AB} = 0$) eV**	**($B = 0.5$, $\Phi_{AB} = 0$) eV**	**($B = 0$, $\Phi_{AB} = 0.5$) eV**	**($B = 0.5$, $\Phi_{AB} = 0.5$) eV**
0	0	−0.5442083329787297	−0.5947495497297974	−0.5462499999999997	−0.5999303898080100
	1	−0.6442083329787298	−0.6947495497297975	−0.6462499999999998	−0.6999303898080100
	2	−0.7475416663120633	−0.7980828830631310	−0.7495833333333333	−0.8032637231413431
	3	−0.8542083329787296	−0.9047495497297973	−0.8562499999999995	−0.9099303898080098
−1	0	−0.5523648181630274	−0.6027415718988567	−0.5462499999999997	−0.5999303898080100
	1	−0.6523648181630275	−0.7027415718988568	−0.6462499999999998	−0.6999303898080100
	2	−0.7556981514963610	−0.8060749052321903	−0.7495833333333333	−0.8032637231413431
	3	−0.8623648181630272	−0.9127415718988565	−0.8562499999999995	−0.9099303898080098
1	0	−0.5523648181630274	−0.6027415718988567	−0.5625224910277047	−0.6158562181041680
	1	−0.6523648181630275	−0.7027415718988568	−0.6625224910277048	−0.7158562181041681
	2	−0.7556981514963610	−0.8060749052321903	−0.7658558243610378	−0.8191895514375012
	3	−0.8623648181630272	−0.9127415718988565	−0.8725224910277045	−0.9258562181041678

Table 3. The generalized pseudo-harmonic oscillator's numerical bound state solution under the influence of the AB and magnetic field with a constant magnetic quantum number but a variable principal quantum number for $\alpha = 0.50$.

m	n	**($B = \Phi_{AB} = 0$) eV**	**($B = 0.5$, $\Phi_{AB} = 0$) eV**	**($B = 0$, $\Phi_{AB} = 0.5$) eV**	**($B = 0.5$, $\Phi_{AB} = 0.5$) eV**
0	0	−0.8171626902482387	−0.8684644504490260	−0.8684644504490260	−0.9345058160807120
	1	−1.3171626902482387	−1.3684644504490260	−1.3684644504490260	−1.4345058160807120
	2	−1.9004960235815722	−1.9517977837823595	−1.9517977837823595	−2.0178391494140455
	3	−2.5671626902482387	−2.6184644504490260	−2.6184644504490260	−2.6845058160807120
−1	0	−1.0163266272276377	−1.0637864531836625	−0.8684644504490260	−0.9345058160807120
	1	−1.5163266272276377	−1.5637864531836625	−1.3684644504490260	−1.4345058160807120
	2	−2.0996599605609716	−2.1471197865169960	−1.9517977837823595	−2.0178391494140455
	3	−2.7663266272276380	−2.8137864531836625	−2.6184644504490260	−2.6845058160807120
1	0	−1.0163266272276377	−1.0637864531836625	−1.2457041729001368	−1.3031582608094352
	1	−1.5163266272276377	−1.5637864531836625	−1.7457041729001368	−1.8031582608094352
	2	−2.0996599605609716	−2.1471197865169960	−2.3290375062334703	−2.3864915941427687
	3	−2.7663266272276380	−2.8137864531836625	−2.9957041729001370	−3.0531582608094350

4.2. Partition Function

Figure 1 presents plots of the $Z(\beta)$ for a generalized pseudo-harmonic oscillator as functions of temperature (T), external magnetic (B), the AB flux, and the screening parameter α. In Figure 1a, we illustrate the $Z(\beta)$ versus temperature at $B = 0.5T$ and $\Phi_{AB} = 0.5$, with different screening parameter values $\alpha = 0.01$, 0.1, and 1.0, respectively. The $Z(\beta)$ declines when screening parameters are increased at fixed values of temperature, the magnetic field, and the AB flux. At a lower temperature T less than 10 K, the three curves moved away from each other, and the lower screening parameter has a higher $Z(\beta)$ compared to those with the higher screening parameter, as can be seen in Figure 1a. Figure 1b illustrates how the $Z(\beta)$ changes in response to a magnetic field at a constant temperature and AB flux for different values of the screening parameter. Here, the $Z(\beta)$ increases as the screening parameter rise alongside the magnetic field. One can also observe in Figure 1b that the curves were linear with almost zero $Z(\beta)$, but as the magnetic field is increased above $20T$, the three curves separated away from each other. This demonstrates the linearly increasing $Z(\beta)$ and above the magnetic field of $20T$, the $Z(\beta)$ increases monotonically with increasing magnetic field $B(T)$. The plot of the $Z(\beta)$ versus AB field for $T = 1.0$ K, $B = 0.5T$ and several values of the screening parameter $\alpha = 0.05$, 0.08, and 0.1 is shown in Figure 1c. Figure 1c displays the dependence of the $Z(\beta)$ on the AB flux for a fixed temperature and magnetic field, demonstrating a decrease as the screening parameter rises. It is observed that the low screening parameter has a higher $Z(\beta)$ as seen in Figure 1c. Figure 1d is the plot of the $Z(\beta)$ versus the screening parameter for $B = 0.5T$, $\Phi_{AB} = 0.5$ and various temperature values $T = 1.0$ K, 2.0 K, and 3.0 K. Figure 1d shows the behaviour of $Z(\beta)$ versus the screening parameter at fixed magnetic and AB fields, indicating a decrease in the $Z(\beta)$ as temperature increases and the screening parameter rises. These figures collectively highlight the complex interplay between temperature, external fields and screening parameters on the $Z(\beta)$ of the generalized pseudo-harmonic oscillator. Finally, Figure 1d shows that the $Z(\beta)$ decreases monotonically with the increasing screening parameter with the conditions $B = 0.5T$, $\Phi_{AB} = 0.5$ and various temperature values $T = 1.0$ K, 2.0 K, and 3.0 K.

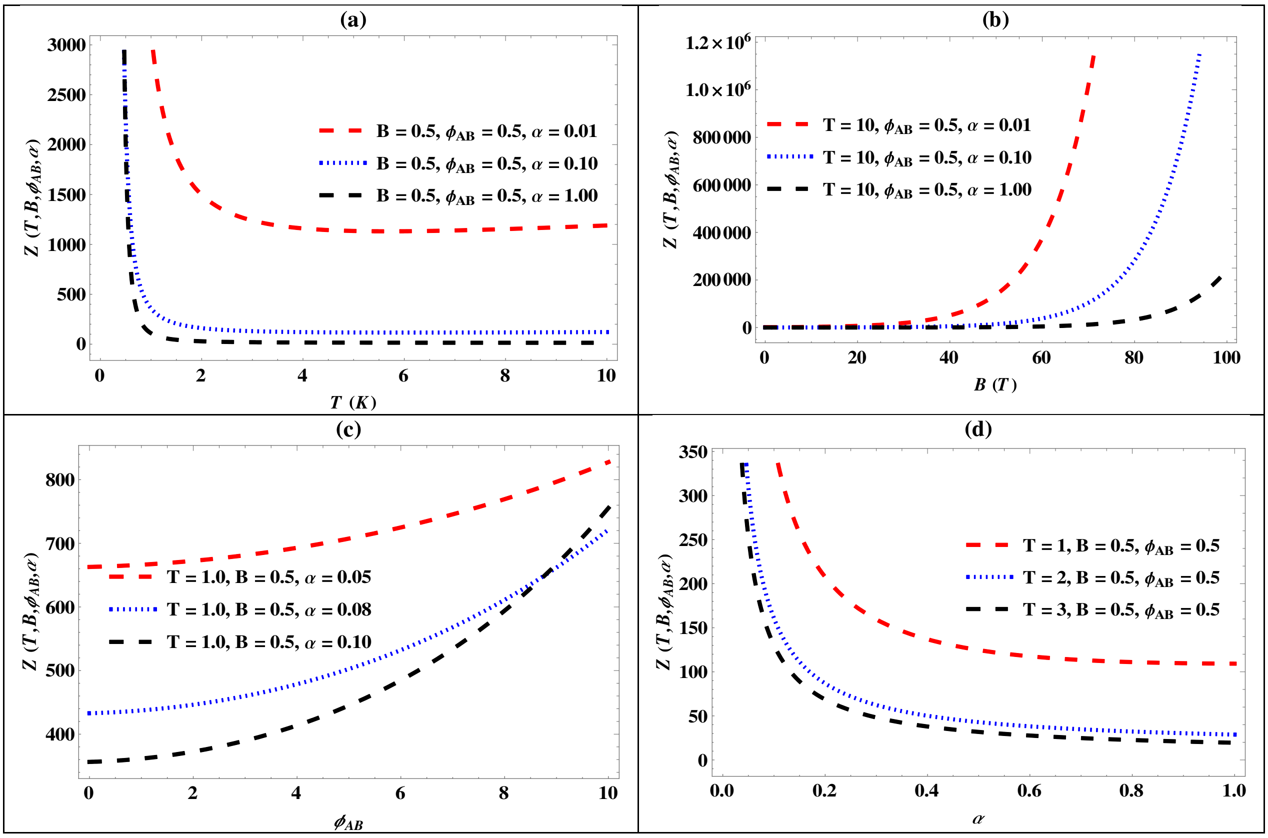

Figure 1. The variation of the Z(β) for the generalized pseudo-harmonic oscillator against (**a**) temperature for different values of the screening parameter (α); (**b**) the magnetic flux $B(T)$ for different values of the screening parameter (α); (**c**) the AB flux (Φ_{AB}) for different values of the screening parameter (α); and (**d**) the screening parameter (α) for different values of temperature (T).

4.3. Helmholtz Free Energy

Figure 2a–d present the plots depicting the Helmholtz free energy versus temperature (T), the magnetic field (B), the AB flux (Φ_{AB}), and the screening parameter (α). In Figure 2a, the Helmholtz free energy increases with rising screening parameters at increasing temperatures. Figure 2b shows how the Helmholtz free energy varies with the magnetic field for a fixed temperature and AB flux, highlighting that an increase in the screening parameter leads to higher free energy as the magnetic field rises. Figure 2c presents the relationship between the Helmholtz free energy and AB flux for a constant temperature and magnetic field, demonstrating an increase in free energy with increasing screening parameters. Figure 2d depicts the variation of free energy with screening parameters at a constant temperature and AB flux for different magnetic field strengths, indicating a decrease in free energy as the magnetic field intensity rises. These figures collectively depict the dependencies of the Helmholtz free energy on temperature, the magnetic field, the AB flux, and the screening parameter, which provides insights into the thermodynamic properties of the system under investigation.

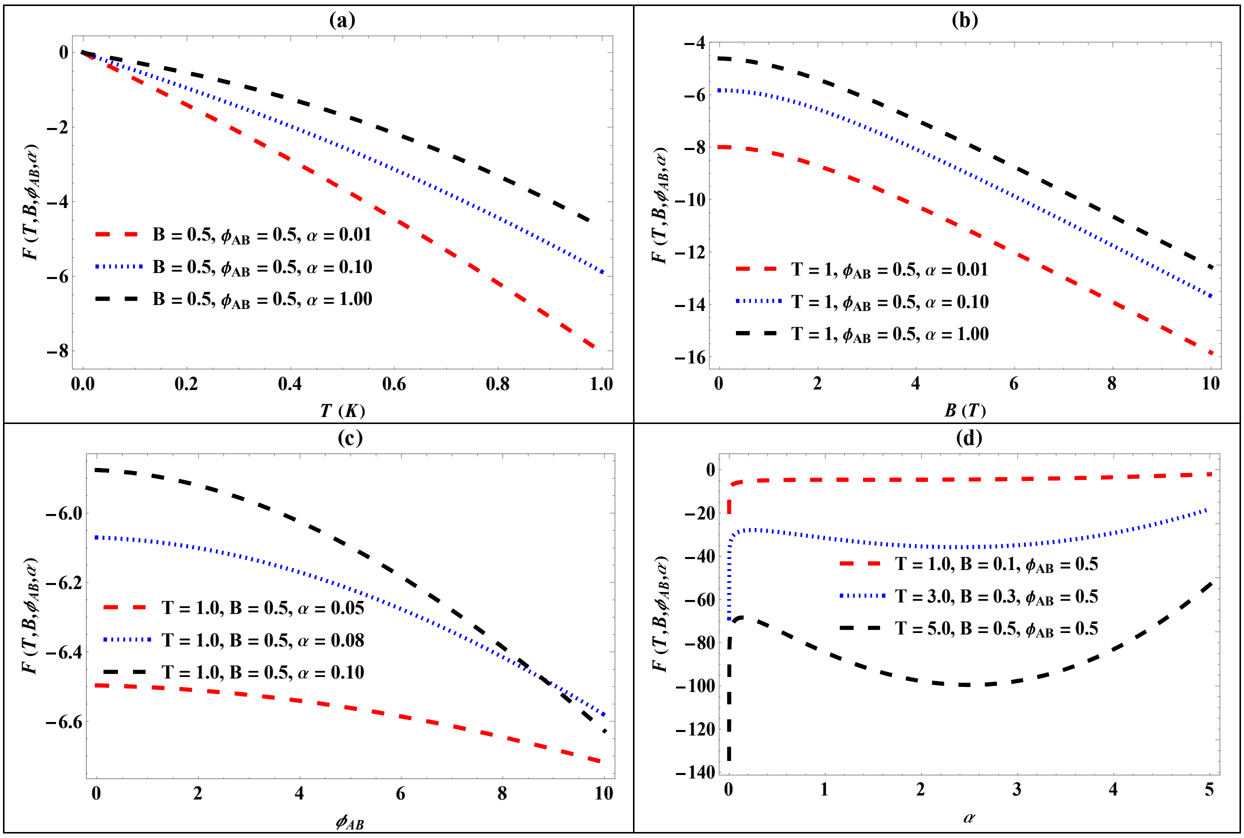

Figure 2. The plot of free energy for the generalized pseudo-harmonic oscillator against (**a**) temperature for different values of the screening parameter (α); (**b**) the magnetic flux $B(T)$ for different values of the screening parameter (α); (**c**) the AB flux (Φ_{AB}) for different values of the screening parameter (α); and (**d**) the screening parameter (α) for different values of temperature (T).

4.4. Mean Energy

Figure 3a–d displays the variations of the mean energy of a generalized pseudo-harmonic oscillator as functions of temperature, the magnetic field applied externally, the AB flux, and the screening parameter. While the magnetic field and AB flux remain constant, Figure 3a illustrates how the mean energy falls with rising temperature as the screening parameter increases. Figure 3b illustrates the variation of the mean energy with the magnetic field for a fixed AB flux and screening parameter, showing a decrease in the mean energy as the temperature increases alongside the magnetic field. Figure 3c shows the relationship between mean energy and the AB flux at a constant magnetic field and temperature, indicating a decrease in mean energy with increasing screening parameters. Figure 3d depicts the variation of mean energy with screening parameters for a fixed magnetic field and AB flux, showing a diminution in mean energy with a rise in temperature to a minimum screening parameter value, after which it increases with further increases in the screening parameter.

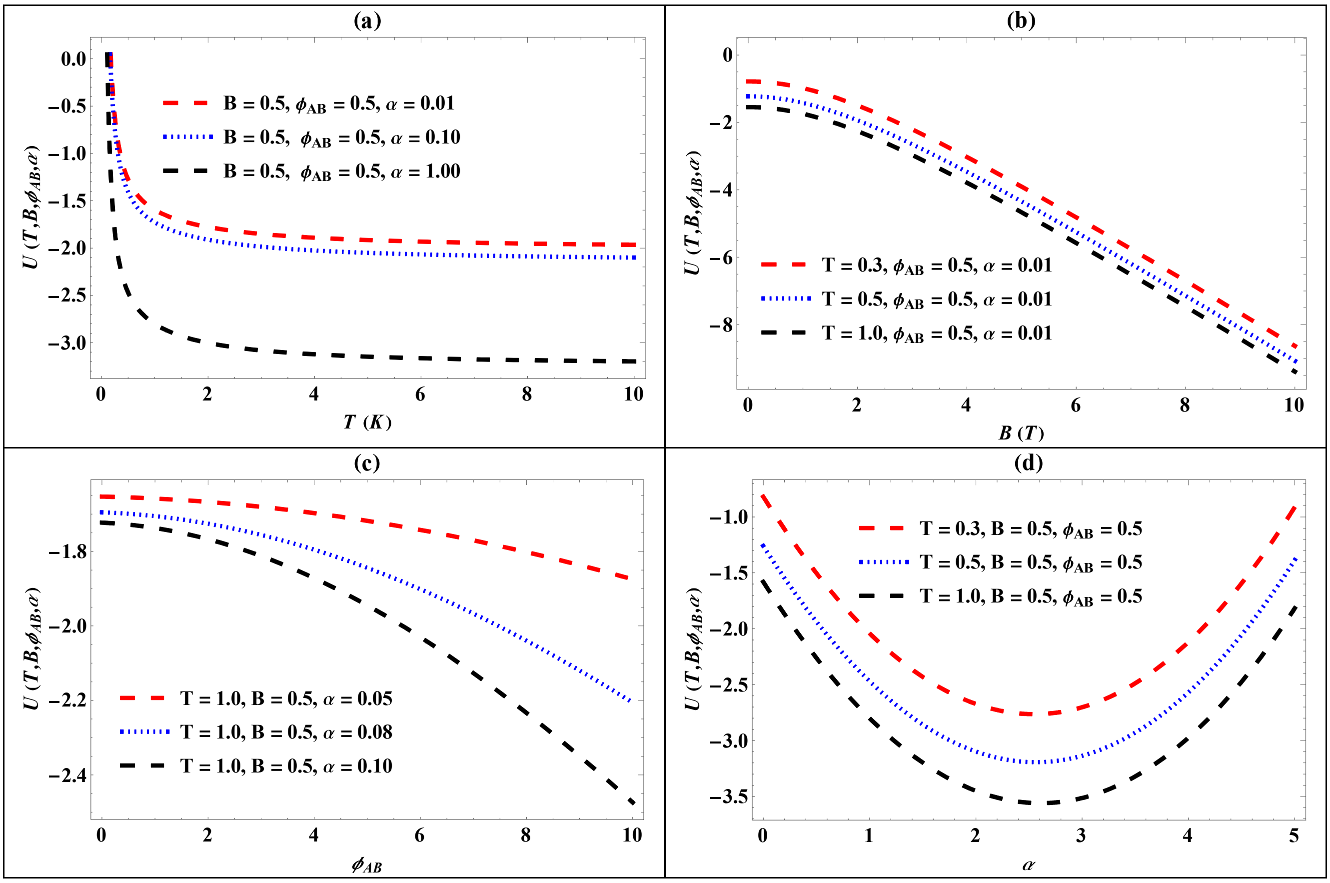

Figure 3. The plot of internal energy for the generalized pseudo-harmonic oscillator against (**a**) temperature for different values of the screening parameter (α); (**b**) the magnetic flux $B(T)$ for different values of the screening parameter (α); (**c**) the AB flux (Φ_{AB}) for different values of the screening parameter (α); and (**d**) the screening parameter (α) for different values of temperature (T).

4.5. Entropy

The entropy plots for the generalized pseudo-harmonic oscillator with varying temperature, external magnetic fields, AB fields, and screening parameters are presented in Figure 4. Figure 4a illustrates the dependence of entropy on temperature at fixed magnetic and AB fields, with varying values of the screening parameter. Increasing the screening parameter correlates with a decrease in entropy for the generalized pseudo-harmonic oscillator. Figure 4b displays the variation of entropy versus magnetic field B for a fixed AB field and screening parameter and varies temperature. In this case, as the magnetic field increases, the entropy rises with a rise in temperature. The plot of the entropy against the AB field for various values of the temperature with a fixed magnetic field and screening parameter is shown in Figure 4c. Under these conditions, a rise in temperature causes an increase in entropy. Figure 4d shows the behavior of the relationship between the entropy and the screening parameter for fixed magnetic and AB fields. By increasing the temperature, an increase in the entropy of the generalized pseudo-harmonic system is observed.

4.6. Specific Heat Capacity

In Figure 5, we show the plots of specific heat capacity versus temperature, the magnetic field, the AB field, and the screening parameter. The variation of the specific heat capacity as a function of temperature is displayed in Figure 5a. It is seen here that the heat capacity increases with an increase in screening parameters for fixed magnetic and AB fields. Figure 5b shows the heat capacity versus the magnetic field for a fixed AB field and screening parameter with varied temperatures. As temperature is increased, the heat capacity decreases under these conditions. The behavior of the heat capacity as a function of the AB field for a fixed magnetic field and the screening parameter for a range of temperature values are displayed in Figure 5c. In this case, the heat capacity decreases with an increase in temperature when the magnetic field and screening parameter are fixed. Figure 5d shows the plot of the heat capacity as a function of the screening for fixed magnetic and AB fields and various temperatures. When the temperature of the system increases under these conditions, the heat capacity of the generalized pseudo-harmonic oscillator decreases also.

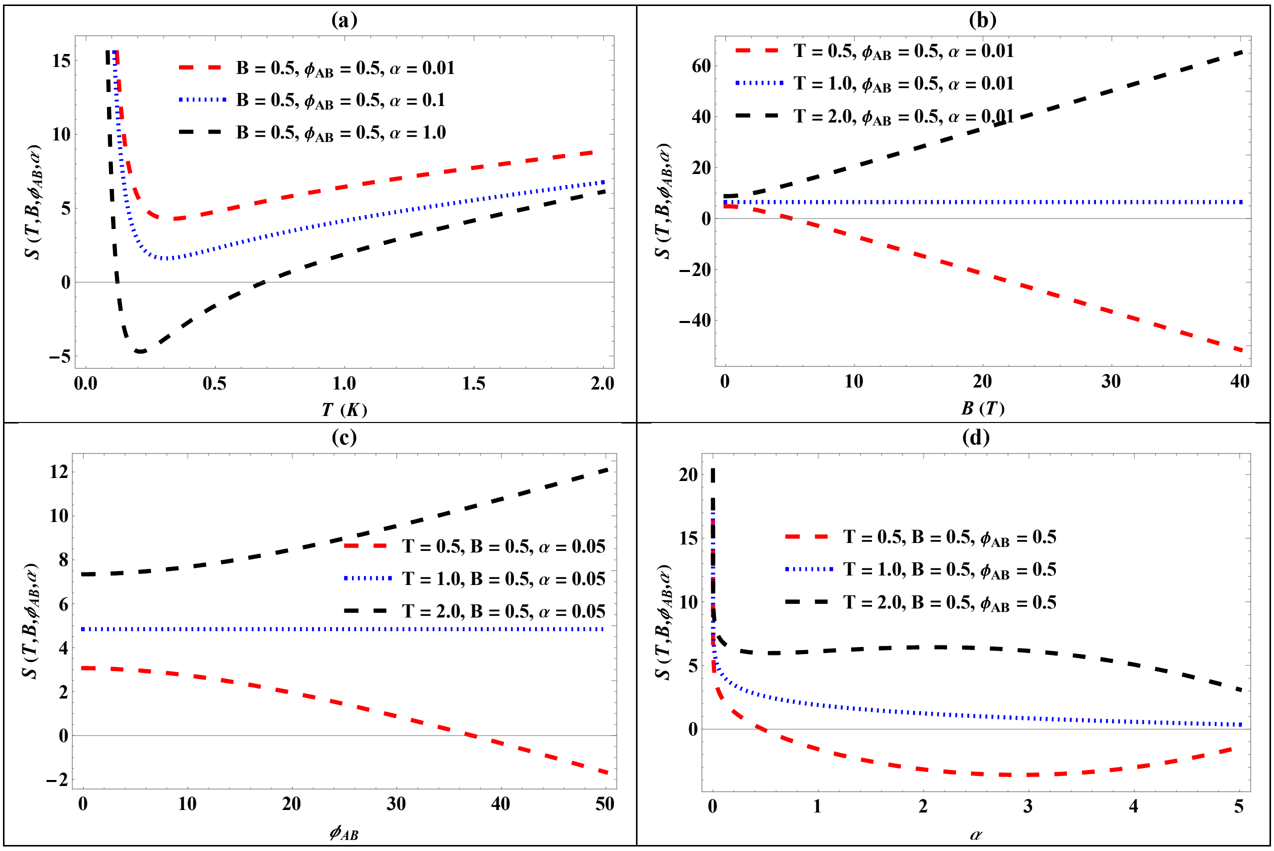

Figure 4. The plot of entropy for the generalized pseudo-harmonic oscillator against (**a**) temperature for different values of the screening parameter (α); (**b**) the magnetic flux $B(T)$ for different values of the screening parameter (α); (**c**) the AB flux (Φ_{AB}) for different values of the screening parameter (α); and (**d**) the screening parameter (α) for different values of temperature (T).

4.7. Magnetization

Figure 6 presents the magnetization of the generalized pseudo-harmonic oscillator across varying parameters, including temperature, the magnetic field, the AB field, and the screening parameter. Figure 6a illustrates the magnetization as a function of temperature, with magnetic and AB fields held constant while varying the screening parameter. In Figure 6b, the plot depicts the magnetization's change in relation to the magnetic field, keeping AB field and screening parameter values fixed. Figure 6c shows the relationship between magnetization and the AB field while maintaining constant values for temperature, the magnetic field, and the screening parameter. Figure 6d explores the dependency of magnetization on the screening parameter, with the magnetic field and AB field held constant. Across Figure 6a–d, it is evident that increasing the screening parameter and temperature under a fixed magnetic field and AB field enhances the magnetization of the generalized pseudo-harmonic oscillator.

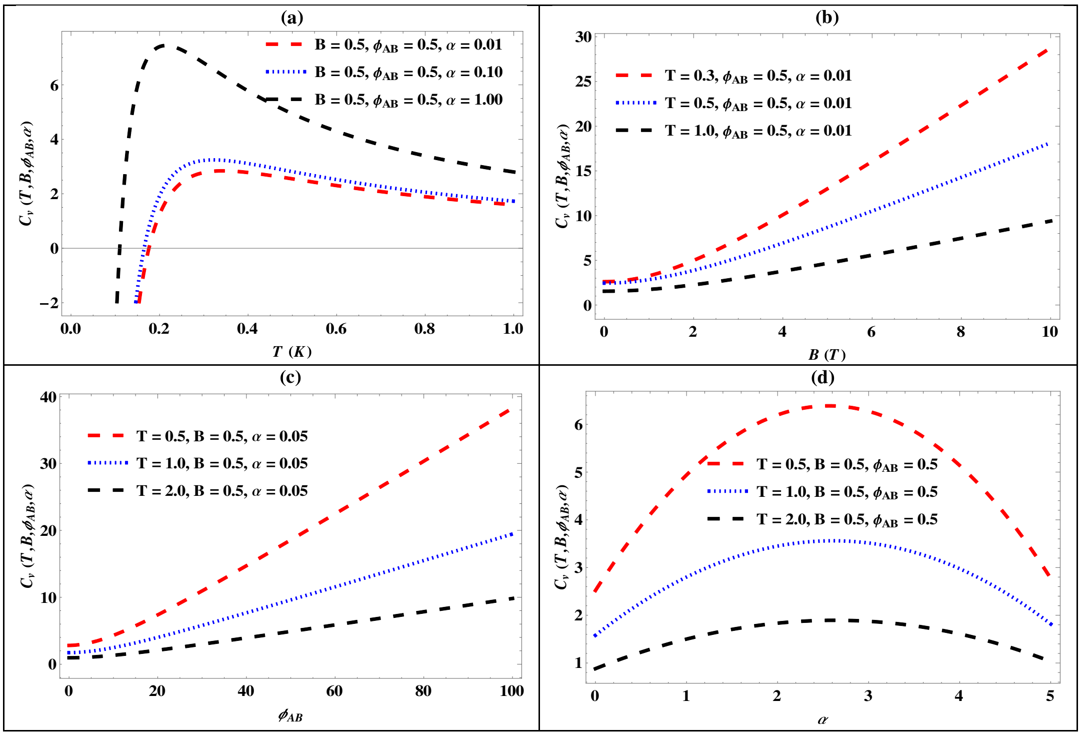

Figure 5. The plot of specific heat capacity for the generalized pseudo-harmonic oscillator against (**a**) temperature for different values of the screening parameter (α); (**b**) the magnetic flux $B(T)$ for different values of the screening parameter (α); (**c**) the AB flux (Φ_{AB}) for different values of the screening parameter (α); and (**d**) the screening parameter (α) for different values of temperature (T).

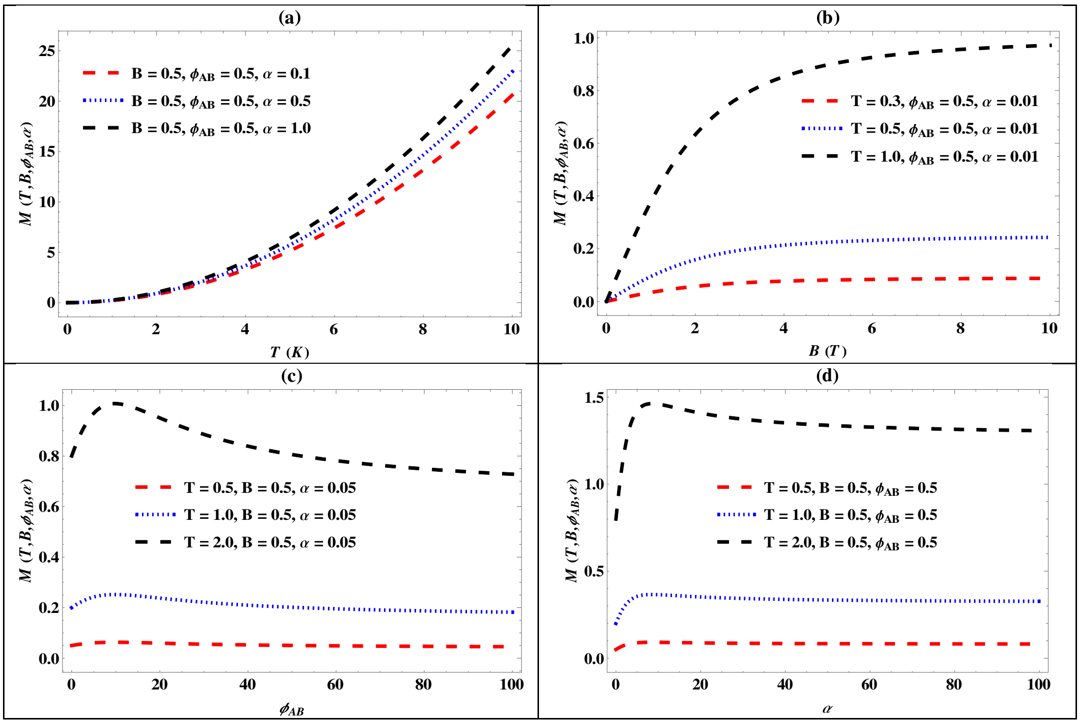

Figure 6. The plot of magnetization for the generalized pseudo-harmonic oscillator against (**a**) temperature for different values of the screening parameter (α); (**b**) the magnetic flux $B(T)$ for different values of the screening parameter (α); (**c**) the AB flux (Φ_{AB}) for different values of the screening parameter (α); and (**d**) the screening parameter (α) for different values of temperature (T).

4.8. Magnetic Susceptibility

Figure 7 depicts the variations in the magnetic susceptibility of the generalized pseudo-harmonic oscillator in relation to temperature, magnetic fields, AB fields, and screening parameters. Figure 7a depicts a plot of magnetic susceptibility against temperature, demonstrating that increasing the screening parameter reduces magnetic susceptibility for fixed magnetic and AB fields. Figure 7b depicts the variation in magnetic susceptibility versus the magnetic field. When the AB and screening parameters are maintained constant, increasing the temperature causes a reduction in magnetic susceptibility, as seen in Figure 7b. Figure 7c depicts a plot of magnetic susceptibility in relation to the AB field. When the magnetic field and screening parameter are fixed, increasing the temperature causes a commensurate rise in magnetic susceptibility. Figure 7d plotted the magnetic susceptibility against the screening parameter. Magnetic susceptibility increases with increasing temperature for constant magnetic and AB fields.

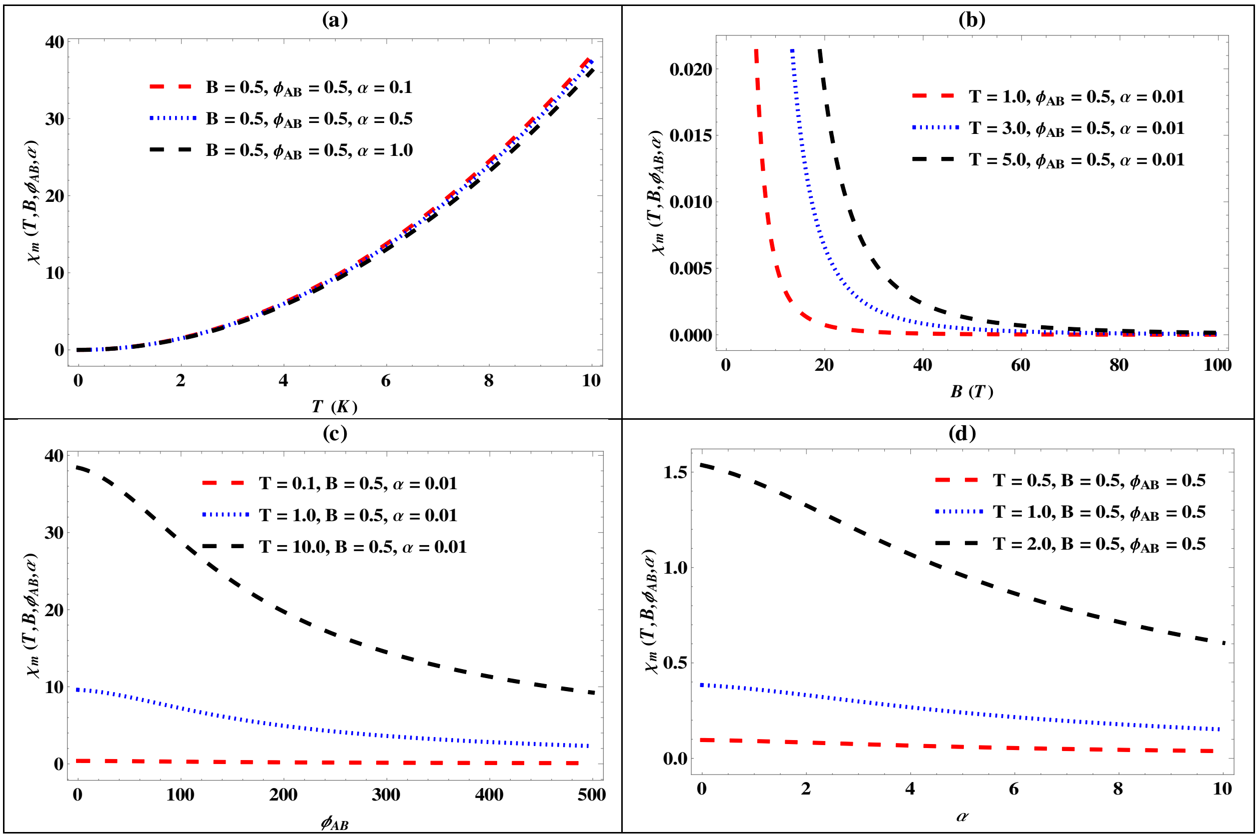

Figure 7. The plot of magnetic susceptibility for the generalized pseudo-harmonic oscillator against (**a**) temperature for different values of the screening parameter (α); (**b**) the magnetic flux $B(T)$ for different values of the screening parameter (α); (**c**) the AB flux (Φ_{AB}) for different values of the screening parameter (α); and (**d**) the screening parameter (α) for different values of temperature (T).

4.9. Persistent Current

Figure 8 illustrates the variations of the persistent current characteristics of the generalized pseudo-harmonic oscillator across varying parameters, including temperature, the magnetic field, the AB field, and the screening parameter. Figure 8a displays the persistent current as a function of temperature, with magnetic and AB fields held constant while the screening parameter varies. In Figure 8b, the plot depicts how the persistent current changes with the magnetic field, maintaining fixed AB field and screening parameter values. Figure 8c illustrates the behavior of the persistent current versus the AB field, with temperature, the magnetic field, and the screening parameter kept constant. Figure 8d examines the relationship between the persistent current and screening parameters while maintaining fixed values for the magnetic field and AB field. Across Figure 8a–d, an increase in both the screening parameter and temperature under fixed magnetic and AB fields results in higher persistent currents for the generalized pseudo-harmonic oscillator.

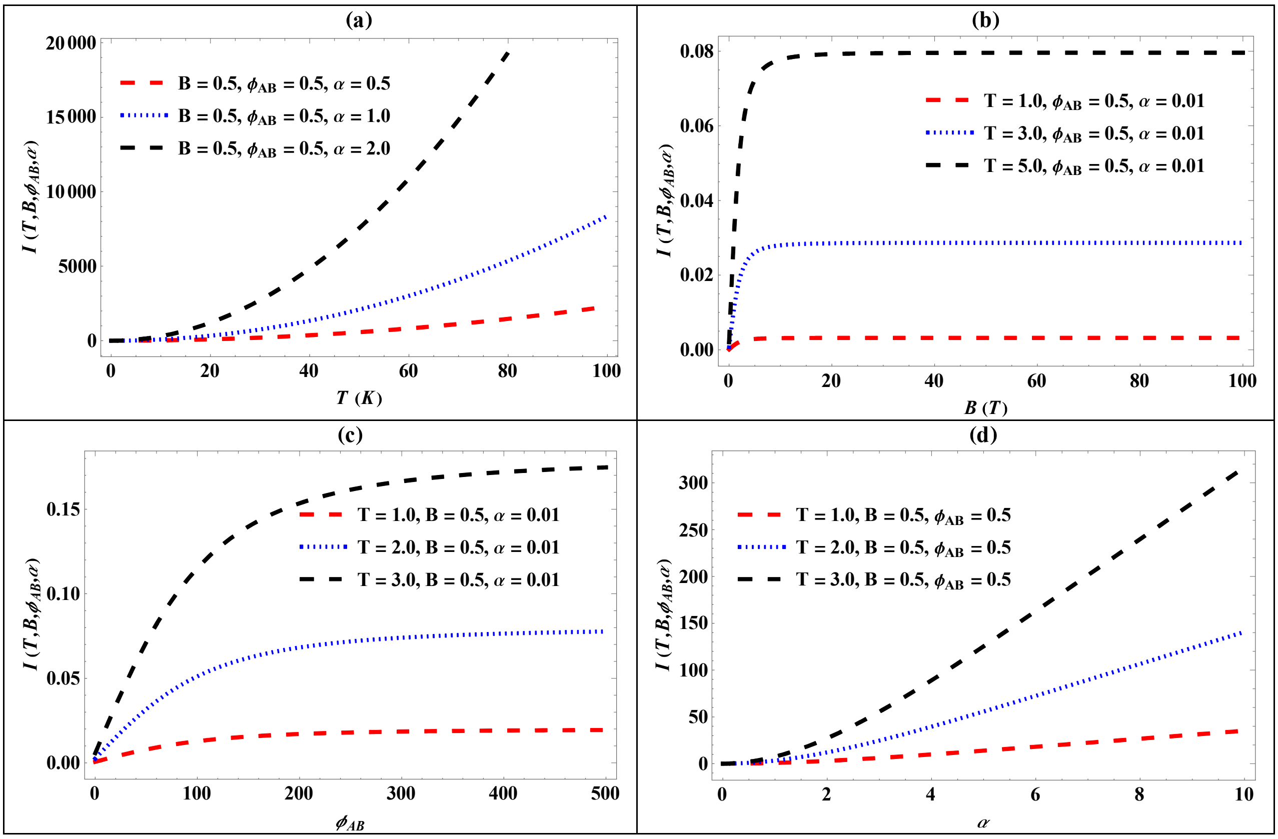

Figure 8. The plot of the persistent current for the generalized pseudo-harmonic oscillator against (**a**) temperature for different values of the screening parameter (α); (**b**) the magnetic flux $B(T)$ for different values of the screening parameter (α); (**c**) the AB flux (Φ_{AB}) for different values of the screening parameter (α); and (**d**) the screening parameter (α) for different values of temperature (T).

5. Conclusions

In this article, the generalized pseudo-harmonic oscillator is studied under the non-relativistic 2D-SE framework. Under specific conditions, this potential simplifies the standard pseudo-harmonic oscillator, which finds diverse applications across various branches of physics. Using the ENU method, we derived the energy spectra and corresponding eigenfunctions stated as a function of confluent Heun functions. Leveraging the energy spectra from Equation (20) and the $Z(\beta)$ given in Equation (29), we conducted a detailed investigation of thermo-magnetic properties, such as free energy $F(\beta)$, internal energy $U(\beta)$, entropy $S(\beta)$, the specific heat capacity C_v (β), magnetization $M(\beta)$, magnetic susceptibility $\chi(\beta)$, and the persistent current $I(\beta)$ for the generalized pseudo-harmonic oscillator. The study systematically examines the influence of temperature and other parameters on these thermo-magnetic properties, employing graphical illustrations to elucidate their dependencies and behaviors. Finally, this investigation is performed within the limit of the minimal coupling for the 2D Schrodinger equation, but recently, the effects of strong coupling to the quantum states have been reported [58–60].

Author Contributions: Conceptualization, H.I.A. and A.N.I.; methodology, R.H. and U.S.O.; software, H.I.A.; validation, R.H., A.N.I. and U.S.O.; formal analysis, R.H. and U.S.O.; investigation, H.I.A. and A.N.I.; writing—original draft preparation, H.I.A. and A.N.I.; writing—review and editing, R.H. and

U.S.O.; visualization, H.I.A. and A.N.I.; supervision, A.N.I.; funding acquisition, H.I.A. All authors have read and agreed to the published version of the manuscript.

Funding: This research was supported by Princess Nourah bint Abdulrahman University Researchers Supporting Project number (PNURSP2024R106), Princess Nourah bint Abdulrahman University, Riyadh, Saudi Arabia.

Data Availability Statement: This manuscript has associated data in a data repository. All data included in this manuscript are available on request by contacting the corresponding author.

Conflicts of Interest: The authors declare no conflict of interest.

References

1. Edet, C.O.; Amadi, P.O.; Onyeaju, M.C.; Okorie, U.S.; Sever, R.; Rampho, G.J.; Abdullah, H.Y.; Salih, I.H.; Ikot, A.N. Thermal Properties and Magnetic Susceptibility of Hellmann Potential in Aharonov–Bohm (AB) Flux and Magnetic Fields at Zero and Finite Temperatures. *J. Low Temp. Phys.* **2021**, *202*, 83. [CrossRef]
2. Rampho, G.J.; Ikot, A.N.; Edet, C.O.; Okorie, U.S. Energy spectra and thermal properties of diatomic molecules in the presence of magnetic and AB fields with improved Kratzer potential. *Mol. Phys.* **2021**, *119*, 5. [CrossRef]
3. Ghosh, P.; Nath, D. Exact solutions and spectrum analysis of a noncentral potential in the presence of vector potential. *Int. J. Quantum. Chem.* **2020**, *120*, e26153. [CrossRef]
4. Mbadjoun, B.T.; Ema, J.M.; Abiama, P.E.; Ben-Bolie, G.H.; Ateba, P.O. Effect of gravity and electromagnetic field on the spectra of cylindrical quantum dots together with AB flux field. *Mod. Phys Lett. A.* **2020**, *35*, 2050092. [CrossRef]
5. Karayer, H. Study of the radial Schrödinger equation with external magnetic and AB flux fields by the extended Nikiforov–Uvarov method. *Eur. Phys. J. Plus.* **2020**, *135*, 70. [CrossRef]
6. Edet, C.O.; Ikot, A.N.; Onyeaju, M.C.; Rampho, G.J.; Lekala, M.L.; Kaya, S. Thermo-magnetic properties of the screened Kratzer potential with spatially varying mass under the influence of Aharanov-Bohm(AB) and position-dependent magnetic fields. *Phys. E* **2021**, *131*, 114710. [CrossRef]
7. Edet, C.O.; Ikot, A.N. Analysis of the impact of external fields on the energy spectra and thermo-magnetic properties of N_2, I_2, CO, NO and HCl diatomic molecules. *Mol. Phys.* **2021**, *119*, 23. [CrossRef]
8. Eshghi, M.; Mehraban, H.; Ikhdair, S. The relativistic bound states of a non-central potential. *Pramana* **2017**, *88*, 73. [CrossRef]
9. Ikot, A.N.; Obagboye, L.F.; Okorie, U.S.; Inyang, E.P.; Amadi, P.O.; Okon, I.B.; Abdel-At, A.-H. Solutions of Schrodinger equation with generalized Cornell potential (GCP) and its applications to diatomic molecular systems in D-dimensions using extended Nikiforov–Uvarov (ENU) formalism. *Eur. Phys. J. Plus* **2022**, *137*, 1370. [CrossRef]
10. Ciftci, H.; Kisoglu, H.F. Nonrelativistic Arbitrary l-States of Quarkonium through Asymptotic Iteration Method. *Adv. High Energy Phys.* **2018**, *4549705*, 1. [CrossRef]
11. Mutuk, H. S-Wave Heavy Quarkonium Spectra: Mass, Decays, and Transitions. *Adv. High Energy Phys.* **2018**, *20*, 653. [CrossRef]
12. Boyacioglu, B.; Chatterjee, A. Dia- and paramagnetism and total susceptibility of GaAs quantum dots with Gaussian confinement. *Phys. E* **2021**, *44*, 1826. [CrossRef]
13. Cetin, A. A quantum pseudodot system with a two-dimensional pseudoharmonic potential. *Phys. Lett. A* **2008**, *372*, 3852. [CrossRef]
14. Ghanbari, A. Rotating effects on the thermophysical properties of a two-dimensional GaAs quantum ring. *Commun. Theor. Phys. Phys.* **2024**, *76*, 065504. [CrossRef]
15. Barke, K. Remarks on a quantum dot described by scalar exponential potentials. *Phys. B* **2024**, *674*, 415590.
16. Li, Y.J. Numerical Calculation of Electronic Structure for Three-Dimensional Nanoscale Semiconductor Quantum Dots and Rings. *Comput. Elect.* **2003**, *2*, 49. [CrossRef]
17. Dong, S.H.; Lozada-Cassou, M.; Yu, J.; Jimenez-Angeles, F.; Rivera, A.L. Hidden symmetries and thermodynamic properties for a harmonic oscillator plus an inverse square potential. *Int. J. Quant. Chem.* **2007**, *107*, 366. [CrossRef]
18. Osobonye, G.T.; Adekanmbi, M.; Ikot, A.N.; Okorie, U.S.; Rampho, G.J. Thermal properties of anharmonic Eckart potential model using Euler–MacLaurin formula. *Pramana* **2021**, *95*, 98. [CrossRef]
19. Okorie, U.S.; Ikot, A.N.; Chukwuocha, E.O.; Rampho, G.J. Thermodynamic properties of improved deformed exponential-type potential (IDEP) for some diatomic molecules. *Res. Phys.* **2020**, *17*, 103078. [CrossRef]
20. Edet, C.O.; Lakaal, K.; El Hamdaoui, J.; Feddi, K.; Perez, L.M.; Feddi, E.; Ikot, A.N.; Ali, N.; Rais, S.A.A.; Asjad, M. Investigating the magneto-transport and thermal properties of 2D electron systems under the influence of the Aharonov–Bohm field and Eckart potential interaction. *Phys. B* **2024**, *673*, 415438. [CrossRef]
21. Ikot, A.N.; Rampho, G.J.; Amadi, P.O.; Sithole, M.J.; Okorie, U.S.; Lekala, M.I. Shannon entropy and Fisher information-theoretic measures for Mobius square potential. *Eur. Phys. J. Plus* **2020**, *135*, 503. [CrossRef]
22. Amadi, P.O.; Ikot, A.N.; Ngiangia, A.T.; Okorie, U.S.; Rampho, G.J.; Abdullahi, H.Y. Shannon entropy and Fisher information for screened Kratzer potential. *Int. J. Quant. Chem.* **2020**, *120*, e26246. [CrossRef]
23. Moreira, A.R.P.; Amadi, P.O.; Horchani, R.; Ikot, A.N.; Ahmed, F. The influence of a magnetic field on Shannon entropy and thermal properties in graphene. *Chin. J. Phys.* **2024**, *89*, 366. [CrossRef]

24. Olendski, O. Quantum information measures of the Aharonov–Bohm ring in uniform magnetic fields. *Phys. Lett. A* **2019**, *383*, 1110. [CrossRef]
25. Amadi, P.O.; Moreira, A.R.P.; Ikot, A.N.; Ali, N.; Aljunid, A.; Horchani, R.J. Effect of the Screening Parameter on Shannon Entropy and Thermal Properties for Exponential Kratzer–Feus Potential. *Low Temp. Phys.* **2024**, *216*, 606. [CrossRef]
26. Kumar, V.; Bhardwaj, S.B.; Singh, R.M.; Chand, F. Optical properties and effect of magnetic field on energy spectra of a GaAs spherical quantum dot. *Eur. Phys. J. Plus* **2023**, *138*, 191. [CrossRef]
27. Hahn, R.V.H.; Mora-Rey, F.; Restrepo, R.L.; Morales, A.L.; Montoya-Sánchez, J.; Eramo, G.; Barseghyan, M.G.; Vinasco, J.A.; Duque, D.A.; Duque, C.A. Electronic and optical properties of tetrapod quantum dots under applied electric and magnetic fields. *Eur. Phys. J. Plus* **2024**, *139*, 311. [CrossRef]
28. Priyanka; Ritu; Kumar, V.; Kumar, R.; Chand, F. First principle calculations to explore the electronic, mechanical and optical properties of 2D NiX2 (X = O, S, Se) monolayers. *Physica B* **2024**, *686*, 415920. [CrossRef]
29. Dvoyan, K.G.; Hayrapetyan, D.B.; Kazaryan; Tshantshapanyan, A.A. Direct Interband Light Absorption in Strongly Prolated Ellipsoidal Quantum Dots' Ensemble. *Nano. Res. Lett.* **2009**, *4*, 2. [CrossRef]
30. Heyn, C.; Duque, C. Donor impurity related optical and electronic properties of cylindrical GaAs-AlxGa1−x As quantum dots under tilted electric and magnetic fields. *Sci. Rep.* **2020**, *10*, 1. [CrossRef]
31. Khordad, R.; Sedehi, H.R.R. Magnetic susceptibility of graphene in non-commutative phase-space: Extensive and non-extensive entropy. *Eur. Phys. J. Plus* **2019**, *134*, 133. [CrossRef]
32. Khordad, R. Second and third-harmonic generation of parallelogram quantum wires: Electric field. *Ind. J. Phys.* **2013**, *87*, 623. [CrossRef]
33. Furtado, C.; Rosas, A.; Azevedo, S. Landau quantization and curvature effects in a two-dimensional quantum dot. *Europhys. Lett.* **2007**, *79*, 57001. [CrossRef]
34. Filgueiras, C.; Rojas, M.; Aciole, G.; Silva, E.O. Landau quantization, Aharonov–Bohm effect and two-dimensional pseudoharmonic quantum dot around a screw dislocation. *Phys. Lett. A* **2016**, *380*, 3847. [CrossRef]
35. Ferkous, N.; Boultif, A.; Sifour, M. On the spin-1/2 Aharonov-Bohm problem for modified Pöschl-Teller potential, physical regularization and self-adjoint extensions. *Eur. Phys. J. Plus* **2019**, *134*, 258. [CrossRef]
36. Bahar, M.K.; Soylu, A.J. Confinement control mechanism for two-electron Hulthen quantum dots in plasmas. *J. Phys. B At. Mol. Opt. Phys.* **2018**, *51*, 105701. [CrossRef]
37. Eshghi, M.; Mehraban, H.; Ikhdair, S.M. Approximate energies and thermal properties of a position-dependent mass charged particle under external magnetic fields. *Chin. Phys. B* **2017**, *26*, 060302. [CrossRef]
38. Ikot, A.N.; Edet, C.O.; Amadi, P.O.; Okorie, U.S.; Rampho, G.J.; Abdullah, H.Y. Thermodynamic properties of Aharanov–Bohm (AB) and magnetic fields with screened Kratzer potential. *Eur. Phys. J. D* **2020**, *74*, 159. [CrossRef]
39. Ikhdair, S.M.; Falaye, B.J.; Hamzavi, M. Nonrelativistic molecular models under external magnetic and AB flux fields. *Ann. Phys.* **2015**, *353*, 282. [CrossRef]
40. Horchani, R.; Al-Aamri, H.; Al-Kindii, N.; Ikot, A.N.; Okorie, U.S.; Rampho, G.J.; Jelassi, H. Energy spectra and magnetic properties of diatomic molecules in the presence of magnetic and AB fields with the inversely quadratic Yukawa potential. *Eur. Phys. J. D* **2021**, *75*, 36. [CrossRef]
41. Khordad, R.; Sedehi, H.R.R. Thermodynamic Properties of a Double Ring-Shaped Quantum Dot at Low and High Temperatures. *J. Low Temp. Phys.* **2018**, *190*, 200. [CrossRef]
42. Vincente, A.G.J.; Castro, L.; Obispo, A.E.; Meza, L.E.A. Remarks on Thermodynamic Properties of a Double Ring-Shaped Quantum Dot at Low and High Temperatures. *J. Low Temp. Phys.* **2021**, *202*, 372. [CrossRef]
43. Elsaid, M.K.; Alia, A.A.; Shaer, A. Rashba spin-orbit interaction effects on thermal and magnetic properties of parabolic GaAs quantum dot in the presence of donor impurity under external electric and magnetic fields. *Chin. J. Phys.* **2020**, *66*, 335. [CrossRef]
44. Ibragimov, G.B. Thermodynamics of quantum wires with a parabolic potential in the tilted magnetic field. *Azerbaijan J. Fizika* **2001**, *9*, 35.
45. Alia, A.A.; Elsaid, M.K.; Shaer, A.J. Magnetic properties of GaAs parabolic quantum dot in the presence of donor impurity under the influence of external tilted electric and magnetic fields. *Taibah Univ. Sci.* **2019**, *13*, 687. [CrossRef]
46. Ikot, A.N.; Okorie, U.S.; Sawangtong, P.; Horchani, H. Effects of Topological Defects and AB Fields on the Thermal Properties, Persistent Currents and Energy Spectra with an Exponential-Type Pseudoharmonic Potential. *Int. J. Theor. Phys.* **2023**, *62*, 197. [CrossRef]
47. Nikiforov, A.F.; Uvarov, V.B. *Special Functions of Mathematical Physics*; Birkhauser: Basel, Switzerland, 1988.
48. Dong, S.H. *Factorization Method in Quantum Mechanics*; Springer: Armsterdam, The Netherlands, 2007.
49. Qiang, W.C.; Dong, S.H. Proper quantization rule. *Eur. Phys. Lett.* **2010**, *89*, 10003. [CrossRef]
50. Ikot, A.N.; Okorie, U.S.; Amadi, P.O.; Edet, C.O.; Rampho, G.J.; Sever, R. The Nikiforov–Uvarov-Functional Analysis (NUFA) Method: A New Approach for Solving Exponential-Type Potentials. *Few-Body Syst.* **2021**, *62*, 9. [CrossRef]
51. Cooper, F.; Khare, A.; Sukhatme, U. Supersymmetry and quantum mechanics. *Phys. Rep.* **1995**, *251*, 267. [CrossRef]
52. Karayer, H.; Demirhan, D.; Buyukkukihc, F.J. Extension of Nikiforov–Uvarov method for the solution of Heun equation. *Math. Phys.* **2015**, *56*, 06350. [CrossRef]
53. Karayer, H.; Demirhan, D.; Buyukkukihc, F. Some special solutions of biconfluent and triconfluent Heun equations in elementary functions by extended Nikiforov-Uvarov method. *Rep. Math. Phys.* **2015**, *76*, 271. [CrossRef]

54. Karayer, H.; Demirhan, D.; Buyukkukihc, F.J. Solution of Schrödinger equation for two different potentials using extended Nikiforov–Uvarov method and polynomial solutions of biconfluent Heun equation. *Math. Phys.* **2018**, *59*, 053501. [CrossRef]
55. Greene, R.L.; Aldrich, C. Variational wave functions for a screened Coulomb potential. *Phys. Rev. A* **1976**, *14*, 2363. [CrossRef]
56. Ronveaux, A. *Heun's Differential Equations*; Oxford University Press: Oxford, UK, 1995.
57. Ikot, A.N.; Okon, I.B.; Okorie, U.S.; Omugbe, E.; Abdel-Aty, A.H.; Obagboye, L.F.; Ahmadov, A.I.; Okpara, N.; Duque, C.A.; Abdullah, H.Y.; et al. Exact solutions of position-dependent mass Schrödinger equation with pseudoharmonic oscillator and its thermal properties using extended Nikiforov–Uvarov method. *Angew. Math. Phys.* **2024**, *75*, 18. [CrossRef]
58. Kaneyasu, M.; Hasegawa, Y. Quantum Otto cycle under strong coupling. *Phys. Rev. E* **2023**, *107*, 044127. [CrossRef] [PubMed]
59. Chen, T.; Balachandran, V.; Guo, C.; Poletti, D. Steady-state quantum transport through an anharmonic oscillator strongly coupled to two heat reservoirs. *Phys. Rev. E* **2020**, *102*, 012155. [CrossRef] [PubMed]
60. Chen, T.; Poletti, D. Thermodynamic performance of a periodically driven harmonic oscillator correlated with the baths. *Phys. Rev. E* **2021**, *104*, 054118. [CrossRef]